J. Fluid Mech. (2000), *vol.* 419, *pp.* 325–344. Printed in the United Kingdom

Prandtl number dependence of Nusselt number in direct numerical simulations

By ROBERT M. KERR AND JACKSON R. HERRING

Geophysical Turbulence Program, National Center for Atmospheric Research, P.O. Box 3000, Boulder, CO 80307, USA

(Received 10 August 1999 and in revised form 8 May 2000)

The dependence of the Nusselt number Nu on the Rayleigh Ra and Prandtl Pr number is determined for $10^4 < Ra < 10^7$ and $0.07 < Pr < 7$ using DNS with no-slip upper and lower boundaries and free-slip sidewalls in a $8 \times 8 \times 2$ box. Nusselt numbers, velocity scales and boundary layer thicknesses are calculated. For Nu there are good comparisons with experimental data and scaling laws for all the cases, including $Ra^{2/7}$ laws at $Pr = 0.7$ and $Pr = 7$ and at low Pr, a $Ra^{1/4}$ regime. Calculations at $Pr = 0.3$ predict a new $Nu \sim Ra^{2/7}$ regime at slightly higher Ra than the $Pr = 0.07$ calculations reported here and the mercury $Pr = 0.025$ experiments.

1. Introduction

It has long been hoped that an unexpected, non-classical scaling law in a simple turbulent flow might lead to a new understanding of turbulent scaling in many systems. Thus, considerable excitement was engendered by the now classic experiment of Heslot, Castaing & Libchaber (1987) who found that the scaling of Nusselt number, Nu, as a function of Rayleigh number (Ra) is better represented by $Nu \sim Ra^{2/7}$ than the previously accepted relation $Nu \sim Ra^{1/3}$. The basis of this proposal was an experiment in He at 7 K, the apparatus being a 1 cm, aspect-ratio 1 cell. In addition to the new scaling, it was proposed that there was a transition from old to new scaling at $Ra > 2 \times 10^7$. Although this particular transition has been called into question, the paper by Heslot *et al.* was the first to indicate that the classical 1/3 law was deficient at very large Ra. The original interpretation of the results depended on observations in a water tank with Prandtl number $Pr = \nu/\kappa = 7$ (Zocchi, Moses & Libchaber 1990), where ν is the viscosity and κ is the thermal diffusivity, and was in terms of large-scale recirculating flow patterns and boundary-layer motions.

However, an experimental result might not lead to a new understanding if it is not universal and depends too strongly on the particular properties of its geometry. Such questions concerning the universality of the 2/7 result have been raised. Most earlier experiments were in wide, flat, large-aspect-ratio boxes using water with Prandtl number $Pr = 7$ (Chu & Goldstein 1973), while the original 2/7 experiments were in small-aspect-ratio cells using a gas with $Pr = 0.7$. The small aspect ratio could be the source of the recirculation pattern and it has long been speculated that varying the Prandtl number could change the scaling laws (Spiegel 1962).

Some of these issues have been addressed with additional experiments and numerical simulations. Fitting $Nu \sim Ra^{\beta_T}$, these have found that $\beta_T < 1/3$ and near 2/7 is ubiquitous, appearing in large-aspect-ratio experiments (Wu & Libchaber 1992)

and simulations (Kerr 1996), with rotation (Julien *et al.* 1996), and even some two-dimensional cases (Deluca *et al.* 1990). Significant velocity boundary layers on the upper and lower surface also seem ubiquitous. Visualizations (Kerr 1996) show the presence of local recirculating patterns and boundary layers even without small aspect ratio or sidewalls. It has even been suggested that in very large-aspect-ratio ($A = W/H = 12$) experiments (Krishnamurti & Howard 1981) that there is evidence for sweeping across the entire domain. The most recent very high Rayleigh number value for β_T in a non-rotating tall cylinder of aspect ratio $A = 0.5$ is $\beta_T = 0.309$ (Niemela *et al.* 2000), a nearly perfect average of the old and new exponent.

This paper addresses the question of the dependence upon Prandtl number. The approach is to assume that both thermal and velocity boundary layers play a crucial role in determining scaling and crossovers and to investigate the scaling properties of boundary layer thicknesses in detail. The reason for believing that velocity boundary layers play a fundamental role stems from the relationship between the scaling of the heat flux and the scaling of a thermal boundary layer λ_T:

$$\lambda_T \sim 1/Nu \sim Ra^{-\beta_T}. \tag{1.1}$$

It has been shown that the classical theory that predicts $Nu \sim Ra^{1/3}$ is equivalent to assuming that all boundary layer thicknesses, temperature and velocity have the same $\lambda \sim Ra^{1/3}$ scaling (Herring 1966). Large-scale motions such as recirculation patterns could create different Ra scalings for boundary layers in velocity λ_u as well as in temperature, and thereby modify the heat flux.

The role of Prandtl number is that the relative values of the thermal and velocity boundary layer thicknesses should depend on the ratio of viscosity to diffusivity, which suggests there that could be crossovers in boundary layer thicknesses as a function of Pr. Such crossovers in length scales are often associated with transitions in scaling behaviour. The possibility of additional transitions first appeared with the theoretical predictions of how the velocity boundary layer would scale with Ra. Shraiman & Siggia (1990) suggested that large-scale flows would be induced by convective heating and assumed that the velocity boundary layer thickness would be equal to the classical viscous boundary layer z^+ and would be greater than the thermal boundary layer thickness, that is $\lambda_u = z^+ > \lambda_T$. They then showed how $Nu \sim Ra^{2/7}$ scaling could be obtained and predicted that $\lambda_u \sim Ra^{-3/7}$ and that $Nu \sim Pr^{-1/7}$. Since $\lambda_T \sim 1/Nu \sim Ra^{-2/7}$, $3/7 > 2/7$, and $\lambda_u > \lambda_T$ for this regime, there should be a crossover at some large critical Ra_c to a regime with $\lambda_u < \lambda_T$. This raised the possibility that some new scaling behaviour would develop.

A competitive theory for the $2/7$ law based upon mixing length and plume generation arguments was proposed by Castaing *et al.* (1989) and has since been refined to address Prandtl number (Cioni, Ciliberto & Sommeria 1997). This theory predicts a velocity boundary layer thickness based upon the estimated thickness of the mixed layer, to be called λ_v, for which $\lambda_v \sim Ra^{-1/7}$. For Pr dependence it predicts $Nu \sim Pr^{-1/7}$ for $Pr > 1$ as before (Shraiman & Siggia 1990) and for $Pr < 1$ it predicts $Nu \sim Pr^{2/7}$. Experiments (Cioni *et al.* 1997) and simulations (Kerr, Herring & Brandenburg 1995; Verzicco & Camussi 1999) do find for $Pr < 1$ a strong increase in Nu between mercury $Pr = 0.025$ and a gas $Pr = 0.7$. A different Ra dependence for mercury, $Nu \sim Ra^{0.25}$, is also found (Cioni *et al.* 1997; Verzicco & Camussi 1999). This debate has continued with new questions about whether the boundary layer for the range of Ra that gives the $2/7$ scaling is truly turbulent (Chavanne *et al.* 1996).

This paper is organized as follows. After defining the equations simulated and the parameter range simulated, the conclusions of previous work on the scaling of

boundary layer thicknesses upon Ra will be discussed. Then the dependence of Nu upon Ra and Pr emerging from the present DNS will be given and the dependence of length scales upon Pr and Ra will be discussed. Crossovers in length scales are found and the effects of these crossovers are discussed and predictions for new crossovers are made. The variation in the scaling exponent of the Nu versus Ra scaling upon Pr and Ra is weak, changing only between approximately 0.25 and 0.28, so as in the previous $Pr = 0.7$ work (Kerr 1996), the primary evidence for crossovers will be in the length scales. Another means to access the importance of the observed crossovers is to relate them to changes in structure, which are discussed in the next section. This work is an extension of an earlier low Rayleigh number study that showed the basic dependence on Pr (Kerr *et al.* 1995) and is consistent with trends in calculations with free-slip upper and lower boundaries (Herring & Jackson 1984).

2. Equations and parameters.

The equations to be solved here are the familiar incompressible Navier–Stokes and temperature advection equations in the Boussinesq limit between two walls:

$$\frac{\partial \boldsymbol{u}}{\partial t} + \boldsymbol{u}\cdot\nabla\boldsymbol{u} = -\frac{1}{\rho_0}\nabla P + T\hat{\boldsymbol{z}} + (1/Re)\nabla^2\boldsymbol{u}, \tag{2.1}$$

$$\frac{\partial T}{\partial t} + \boldsymbol{u}\cdot\nabla T = Pr\nabla^2 T, \tag{2.2}$$

$$\nabla\cdot\boldsymbol{u} = 0. \tag{2.3}$$

No-slip, constant-temperature boundary conditions are used on the upper and lower surfaces and free-slip, zero-flux boundary conditions are used on the sides in a rectangular horizontal domain. The details of the Chebyshev method have been presented before (Kerr 1996), with the addition that sine and cosine transforms now replace Fourier transforms in the horizontal so as to be able to represent sidewall boundary conditions. For these equations the Rayleigh number is

$$Ra = \frac{\alpha Prgd^3\Delta T}{\nu^2}, \tag{2.4}$$

where $\alpha g = 1$, $d = 2$ is the height of the box and $\Delta T = 2$ is the temperature difference across the box. The Nusselt number will be the value obtained from the normalized, volume-averaged heat flux, since this was found to be the most stable definition of Nu (Kerr 1996):

$$Nu = \frac{\overline{wT}}{\kappa\Delta T/d}. \tag{2.5}$$

Given long enough statistical samples this will equal the definition based upon the wall derivative:

$$Nu_w = \frac{\overline{\partial T/\partial z|_w}}{(T_0 - T_1)/d}. \tag{2.6}$$

The Reynolds and Péclet numbers are

$$Re = Ud/\nu, \quad Pe = Ud/\kappa, \tag{2.7}$$

where U is a large-scale velocity that is to be defined.

All the calculations will be for large aspect ratio, $A = 4$, whereas most of the experiments are for small aspect ratio, $A \leqslant 1$. From preliminary work on simulations

	Pr					
Ra	0.07	0.3	0.7	2.0	4.0	7.0
10^4	$64^2 \times 32$	$64^2 \times 32$				$64^2 \times 32$
10^5	$96^2 \times 48$	$96^2 \times 48$				$96^2 \times 48$
4×10^5	$128^2 \times 64$	$128^2 \times 64$				
10^6		$128^2 \times 64$				$128^2 \times 64$
2×10^6	$256^2 \times 128$	$128^2 \times 64$				
4×10^6		$256^2 \times 128$				$192^2 \times 96$
10^7		$256^2 \times 128$	$192^2 \times 96$	$192^2 \times 96$	$256^2 \times 128$	$256^2 \times 128$

TABLE 1. The mesh sizes $nx \times ny \times nz$ for the values of Ra and Pr simulated.

with this code for $A = 1$, $Pr = 0.7$ (Kerr, Brandenburg & Herring 2000), aspect ratio has a noticeable effect upon Nu, recirculation patterns, and velocity profiles only for $A \leqslant 1$. Since tests have shown that the effect of A appears to be insignificant once $A > 2$, in order to concentrate upon the effects of Pr, this paper will consider only $A = 4$ calculations. The results to be given are all from statistical samples of several convective turnover times taken after the simulations had reached a statistically steady state in a manner consistent with previous work (Kerr 1996).

Resolution was chosen to capture the smallest turbulent length scale, either the Kolmogorov scale $\eta = (\nu^3/\epsilon)^{1/4}$ or the Batchelor scale $\eta_B = Pr^{-1/2}\eta$. In the centre of the cell there was roughly equal resolution in the horizontal and vertical with $\Delta x \approx \Delta z \approx 4\min(\eta, \eta_B)$. While the (η, η_B) criterion was designed for resolving the turbulence in the centre of the cell, previous work (Kerr 1996) found that this manner of estimating the resolution also applies to the fine-scale Chebyshev resolution in the boundary layer because $\eta \approx z^+$. The resolution is given in table 1. The maximum Ra for all the Pr cases except $Pr = 0.07$ is 10^7. For $Pr = 0.07$ the maximum Rayleigh number is 2×10^6 because low-Pr convection is more turbulent (higher Reynolds number) with a small Kolmogorov scale. At high Pr, convection is barely turbulent at moderate Ra and η_B determines resolution requirements.

3. Three lengths scales

Each of the two theories for the $Nu \sim Ra^{2/7}$ law that have been mentioned (Shraiman & Siggia 1990; and Castaing *et al.* 1989) predicts that the Reynolds or Péclet number (2.7) should vary as $Ra^{3/7}$ and assume that $\lambda_u > \lambda_T$. To differentiate between the two theories requires determining detailed velocity or kinetic energy profiles as a function of both distance from the walls and Ra. Some velocities have been determined experimentally, finding $\epsilon \approx 0.46 - 0.51$ in $Re \sim Ra^{\epsilon}$ (Sano, Wu & Libchaber 1989), which is slightly greater than the $3/7 \approx 0.43$ predictions and is marginally closer to the classical prediction of $4/9 \approx 0.44$. However, flow visualization is difficult in a gas, so detailed velocity profiles have so far eluded the experimentalists. One attempt has been made to determine some sort of velocity boundary layer thickness from cutoffs of temperature frequency spectra (Belmonte, Tilgner & Libchaber 1994). It can be shown (Kerr *et al.* 1995) that this indirect measurement is not directly related to any of the boundary layer thicknesses to be discussed.

In numerical simulations, full velocity fields are available and vertical profiles can

be used to find a variety of boundary layer thicknesses. This was taken advantage of in the analysis of a series of three-dimensional simulations for $Pr = 0.7$ on meshes as large as $288 \times 288 \times 96$ (Kerr 1996). The velocity boundary layer thickness was determined by three methods. First, from the wall derivative,

$$z^+ = \left(\frac{\nu}{\langle (\partial u/\partial z)^2 \rangle^{1/2}} \right)^{1/2}, \tag{3.1}$$

where a root-mean stress must be used because without a mean flow, the mean shear $\langle \mathrm{d}u/\mathrm{d}z \rangle = 0$. The second is $z^* \sim 1/Re$. (Our definition here of z^* is independent of the question of whether the flow is turbulent: see also the discussion of this quantity in Kerr 1996.) And third, λ_u, which is the peak position of the horizontal kinetic energy profiles. In a classical momentum boundary layer, all of the velocity boundary layer thicknesses, z^+, z^* and λ_v, scale with Reynolds number in the same manner (Kim, Moin & Moser 1987). The present DNS indicate that this is not the case with convection. Instead, z^* and z^+ were found to be nearly the same and scale as one prediction, $(z^*, z^+) \sim Ra^{-3/7}$, and λ_u scaled as the other prediction $\lambda_u \sim Ra^{-1/7}$. Furthermore, while $\lambda_u > \lambda_T$ as the theories assumed, it was found that $(z^*, z^+) < \lambda_T$. Since the highest Ra is definitely in the $2/7$ regime for large-aspect-ratio experiments (Wu & Libchaber 1992), the satisfying aspect of this discovery is that it implies that there will be no further crossovers since $z^+ < \lambda_T$ already is found.

Thus, the asymptotic high Rayleigh number regime for $Pr = 0.7$ suggested by these simulations is one with three boundary layer thicknesses where $z^+ < \lambda_T < \lambda_u$, with Ra scaling exponents of approximately $-3/7$, $-2/7$, and $-1/7$ respectively. This separation in length scales was the primary evidence used to support the $Nu \sim Ra^{2/7}$ scaling in the earlier numerical work (Kerr 1996), since the difference between $1/3$ and $2/7$ was not discernable in the numerical presentation of Nu vs. Ra found there. This will again be the case here, with the statistical error for β_T typically $\delta\beta_T \sim 0.02$ as before (Kerr 1996). Therefore trends in β_T, not particular values, will be emphasized, and for economy of presentation we do not show error bars here; the margins of error for one dimension are the same as in Kerr (1996).

One of the questions this paper tries to address is whether the order of the boundary layer length scaling (i.e. $z^+ < \lambda_T < \lambda_u$) is a requirement for $2/7$. It will be shown that for some Pr there are Ra regimes where $z^+ < \lambda_T < \lambda_u$ is not found. For a given value of Pr, does this lead to different Ra^{β_T} behaviour for Nu? And over the range of Ra where $z^+ < \lambda_T < \lambda_u$ is found, does this invariably lead to $Nu \sim Ra^{2/7}$ behaviour? If so, this would support the suggestion (Kerr 1996) that once $z^+ < \lambda_T < \lambda_u$ appears, $Nu \sim Ra^{2/7}$ is the asymptotic high Rayleigh number scaling.

4. Nu vs. Ra for three Pr values

The current interest in Rayleigh–Bénard convection stems from the scaling and transitions in Nusselt number, whose dependence upon Ra and Pr is given in figure 1 and discussed in this section. Nusselt number is plotted as a function of Ra for $Pr = 0.07$, 0.3 and 7 and as a function of Pr for $Ra = 10^7$ for these Pr and in addition $Pr = 0.7$, 2 and 4. Nu vs. Ra for $Pr = 0.7$ is not shown because the curves are almost identical to those already published (Kerr 1996) and because the major points to be made here are similar, but more obvious, for $Pr = 0.3$.

Dashed lines have been drawn in figure 1(*a–c*) for comparison with the experimental and predicted Nusselt number dependences. In figure 1(*a*) for $Pr = 0.07$, the fit is

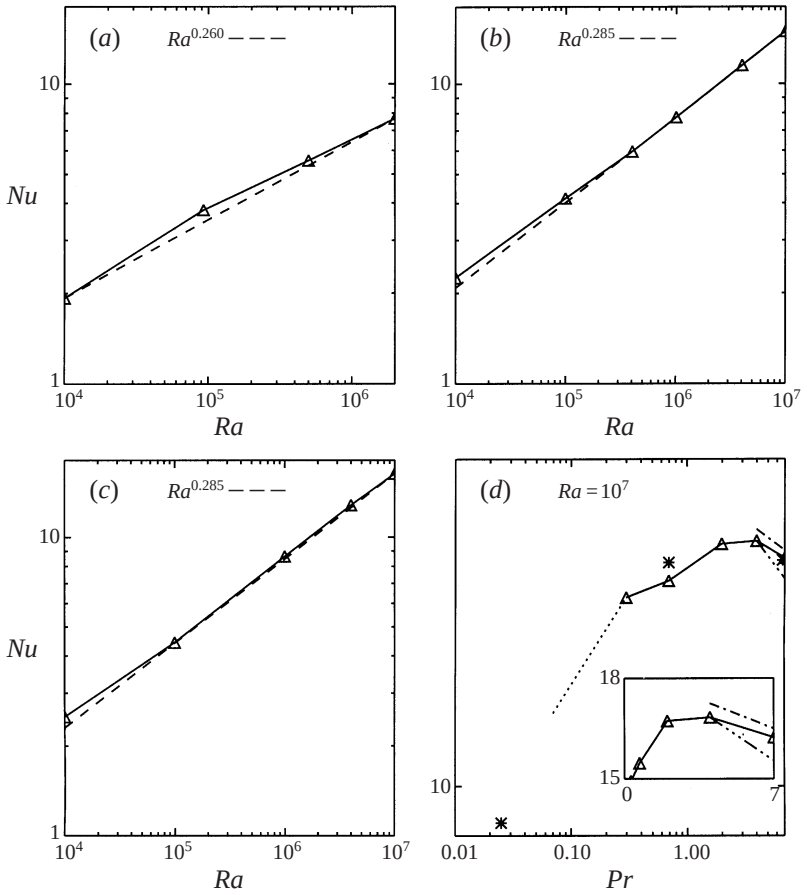

FIGURE 1. Nu vs. Ra and Pr. (a–c) Nu vs. Ra for $Pr = 0.07$, 0.3, and 7.0. The β_T in $Nu = Ra^{\beta_T}$ are given. Triangles indicate where there is numerical data. Dashed lines are the power laws plotted for each Pr. (d) Nu vs. Pr for $Ra = 10^7$. The inset is a blowup of the $Pr \geqslant 0.7$ regime on linear axes. The dotted line in (d) is the value of Nu for $Pr = 0.07$ and $Ra = 10^7$ as extrapolated from (a). Stars indicate experimental values at $Pr = 0.025, 0.7$ and 7. Dot-dashline is the experimental curve from Liu & Ecke (1997). Triple-dot-dashline is the $Pr^{-1/7}$ prediction of Shraiman & Siggia (1990). All calculations are in a $8 \times 8 \times 2$ box with no-slip, constant-temperature top/bottom and free-slip, insulating sidewalls.

$Nu \sim Ra^{0.26}$, consistent with recent experiments for mercury (Cioni *et al.* 1997) with $Pr = 0.025$ up to $Ra = 10^9$, where in $Nu \sim Ra^{\beta_T}$, $\beta_T = 0.25$ and not $2/7 \approx 0.285$ over a sufficiently long range of Ra so as to be convincing. The value of Nu for $Pr = 0.07$ and $Ra = 10^7$ used in figure 1(d) is obtained by extrapolating the $Nu \sim Ra^{0.26}$ trend in figure 1(a) to $Ra = 10^7$. Slight changes in this power law would not affect the primary trends with Pr that will be discussed.

In figure 1(b), $Pr = 0.3$, a $Nu \sim Ra^{0.285}$ dashed line is drawn. This is the fit for $Ra = 4 \times 10^5$ to 10^7. However, for $Ra < 4 \times 10^5$, the slope is noticeably less. For $Ra = 10^5$ to 4×10^5, $Nu \sim Ra^{0.26}$. In figure 1(c), $Pr = 7$, a $\beta_T = 0.285$ dashed line is drawn again. And again it is only a partial fit for Ra between 4×10^5 and 10^7. The dependence of Nu on Ra will be returned to below.

Figure 1(d) plots Nu for $Ra = 10^7$, with the value for $Pr = 0.07$ at $Ra = 10^7$ the extrapolated value from figure 1(a). Also plotted are a number of direct and

extrapolated experimental values. These include experimental values from mercury $Pr = 0.025$ with $Nu = 9.24$ (Cioni *et al.* 1997), large-aspect-ratio gas $Pr = 0.7$ (Wu & Libchaber 1992) and water $Pr = 6.7$ (Chu & Goldstein 1973). The experimental values for $Pr = 4$ to 7 at $Ra = 10^7$ are extrapolated from gaseous helium experiments (Liu & Ecke 1997) at higher Ra assuming a 2/7 dependence on Ra.

The simulations are in good agreement with the experimental trends. Where details are different from the conclusions of earlier experimental work, this is mainly due to more values of Pr than before. The peak in Nu versus Pr is near $Pr = 2$, which would suggest that Pr is not a major factor in recent experiments where Pr was allowed to vary between 1 and 2 as one way of increasing the Rayleigh number (Chavanne *et al.* 1996; Niemela *et al.* 2000). There is a strong increase in Nu with Pr for $Pr < 0.7$, consistent with the experimental Nu for mercury $Pr = 0.025$. A power law of $Nu \sim Pr^{0.12}$ fits the data between $Pr = 0.07$ and 0.7. The experimental fit cited by Cioni *et al.* (1997) is $Pr^{0.21}$, although the fit between the two experimental points at $Pr = 0.025$ and $Pr = 0.7$ at $Ra = 10^7$ shown is $Pr^{0.16}$. This and the present numerical results would be consistent with the numerical fit of $Pr^{0.14}$ of Verzicco & Camussi (1999).

For $2 < Pr < 7$ there is a gradual decrease of Nu with increasing Pr in good agreement with the $Pr = 4$ to 7 helium data from Liu & Ecke (1997) and now also data from Niemela *et al.* (2000). Both these simulations and the helium data find a weaker decrease with Prandtl number than the predicted $Pr^{-1/7}$ scaling shown in figure 1(*d*) (Shraiman & Siggia 1990). A trend similar to this has now been observed experimentally up to $Pr = 300$ (Ashkenazi & Steinberg 1990). To investigate this further, simulations with $Pr = 20$ at sufficiently high Ra are feasible. There are also experimental data for an electrochemical analogue to convection (Goldstein, Chiang & See 1990) at a very high Prandtl number of 2000 with a Nusselt number that would be consistent with the line of zero slope drawn between $Pr = 0.7$ and 7. The Reynolds number at such a value of Pr would be very small and while the flow might exhibit temporal chaos on a long time scale, it would not be turbulent and therefore might not be relevant to the discussions here. To investigate this regime with simulations, one could take the $Pr \to \infty$ limit where the advection term for the velocity in (2.1) is eliminated and assume that the velocity is determined by

$$\nu \nabla^2 \boldsymbol{u} = \nabla p + \hat{\boldsymbol{g}} \theta \tag{4.1}$$

(see e.g. Herring 1969).

Many of these scaling trends could be consistent with new theoretical work by Lohse & Grossman (2000) that divides the parameter space of Pr and Ra into several regimes. In particular the low-Pr regime where $Nu \sim aRa^{1/4} + bRa^{1/3}$ is predicted. The basis for their model is an assumption that the dissipation in the boundary layer is laminar while the dissipation in the bulk is turbulent. Figures 3 and 4 below show sharp gradients in the horizontal velocity profiles near the walls, while previous work for $Pr = 0.7$ (Kerr 1996) shows a sharp rise in the dissipation near the wall so that a large fraction (about 1/4) of the total turbulent dissipation is in the boundary layer. Whether the boundary layer is turbulent or laminar is currently being investigated more carefully.

5. Observed length scales

To understand what crossovers could be occurring in the Nu vs. Ra plots in figure 1, it is necessary to look at the three boundary layer thicknesses z^*, λ_T, and λ_u defined

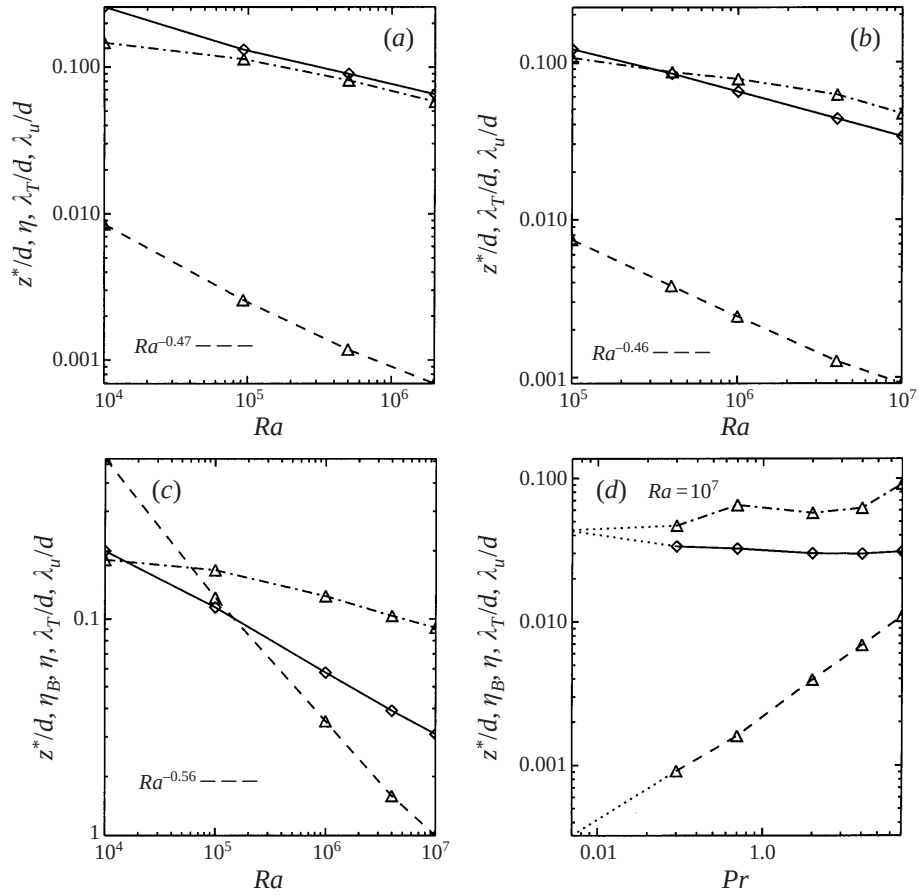

FIGURE 2. Length scales vs. Ra and Pr. (a–c) Length scales vs. Ra for $Pr = 0.07$, 0.3, and 7.0. Dashed line, triangles is $z^* = 1/Pe$ from the prediction based upon classical velocity boundary layer theory (Shraiman & Sigga 1990). Solidline, diamonds is $\lambda_T/d = 0.5/Nu$. Dot-dashline, triangle is λ_u, the position of the peak of the horizontal kinetic energy profiles such as in figures 3 and 4 and is related to the prediction of mixing length theory (Castaing *et al.* 1989). The ϵ in $z^*/d = (Pr/Re) = Ra^{-\epsilon}$ are given. (d) Shows z^*, λ_T and λ_u at $Ra = 10^7$. Dotted lines represent the continuation to extrapolated values for $Pr = 0.07$ and $Ra = 10^7$.

around (3.1). These are plotted for $Pr = 0.07$, 0.7 and 7 in figure 2(a–c), with figure 2(d) plotting their values for all Pr for $Ra = 10^7$. Figures 3 and 4 plot vertical temperature and velocity profiles for $Pr = 0.07$ and 7 for the highest Ra in each case to determine whether the profiles are similar enough to the previous $Pr = 0.7$ case (Kerr 1996) for z^*, λ_T, and λ_u to have the same meanings. The profiles plotted are the root-mean velocities,

$$U_{h\_rms}, W_{rms} = (\overline{u^2})^{1/2}, (\overline{w^2})^{1/2}, \tag{5.1}$$

the temperature variances $T'_{rms} = (\overline{T'^2})^{1/2}$, the mean temperatures $T = \overline{T(z)}$, and mean horizontal velocities $U_h = \overline{u}$. Kinetic energies can be found by taking $U^2_{h\_rms}, W^2_{rms}$ and Reynolds numbers can be determined by taking $Re = (U_{h\_rms}, W_{rms})d/\nu$. The values used in figure 2 are taken from long time averages, while the profiles in figures 3 and 4 are for only one time, averaged in horizontal planes and direction.

As was observed for $Pr = 0.7$ (Kerr 1996), for both $Pr = 0.07$ and $Pr = 7$ the

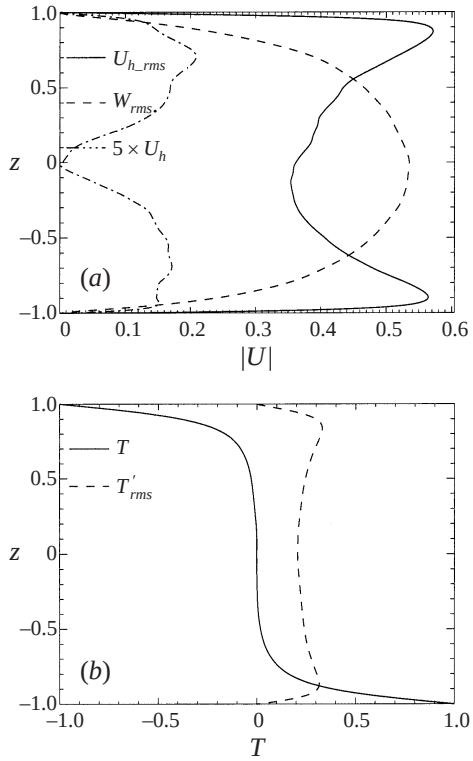

FIGURE 3. Profiles of (*a*) root-mean velocities U_{h_rms}(——), W_{rms}(− − −) = $(\overline{u^2})^{1/2}, (\overline{w^2})^{1/2}$, and the mean horizontal velocity $U_h = |\overline{u}|$(− · −) in the direction of maximum mean flow; (*b*) temperature variance $T'_{rms} = (\overline{T'^2})^{1/2}$(− − −) and temperature $\overline{T}$(———) for a single time for the $Pr = 0.07$, $Ra = 2 \times 10^6$.

profile of W_{rms} peaks in the centre and there is a peak near the boundary in the U_{h_rms} profile that can be used to define λ_u. The profile of T'_{rms} has a peak near the boundary whose thickness scales with Ra the same way as the definition of a thermal boundary layer thickness based on the wall derivative or Nusselt number in (2.6). Therefore, the definitions of z^*, λ_T, and λ_u are the same as before. The mean velocity profiles are discussed below.

The scaling of z^*, λ_T, and λ_u with Ra in figure 2 is also similar to the $Pr = 0.7$ case, with some small but possibly significant differences. By definition, the exponents of $z^* \sim 1/Re = Ra^{-\epsilon}$, can be found from Reynolds numbers. Using the Reynolds number formed by taking either the peaks of W_{rms} or U_{h_rms}, previous numerical and experimentally work has found that $\epsilon \sim 0.46$ to 0.54. For $Pr = 0.07$ and 0.3, $\epsilon \approx 0.46$ in figure 2, which is consistent with the previous $Pr = 0.7$ numerical results (Kerr 1996). For $Pr = 7$, $\epsilon = 0.56$, which while surprisingly large, is consistent with two-dimensional simulations for $Pr = 7$ for which $\epsilon = 0.54$ (Werne *et al.* 1991). Since $\lambda_T \sim 1/Nu$, $\lambda_T \sim Ra^{-\beta_T}$ with $\beta_T = (0.25 - 0.28)$. And if $\lambda_u \sim Ra^{-\beta_u}$, then $\beta_u \approx 1/7$ as before so that $\beta_u < \beta_T < \epsilon$ for all of the Prandtl numbers.

What does figure 2 tell us about the ordering and scaling of the three boundary layer thicknesses for different Ra for the three Pr? Recall that $Nu \sim Ra^{2/7}$ scaling was associated with $z^* < \lambda_T < \lambda_u$ in the $Pr = 0.7$ work (Kerr 1996). For $Pr = 0.07$, the ordering for all Ra is $z^* < \lambda_u < \lambda_T$ and figure 2(*d*) would be consistent with this

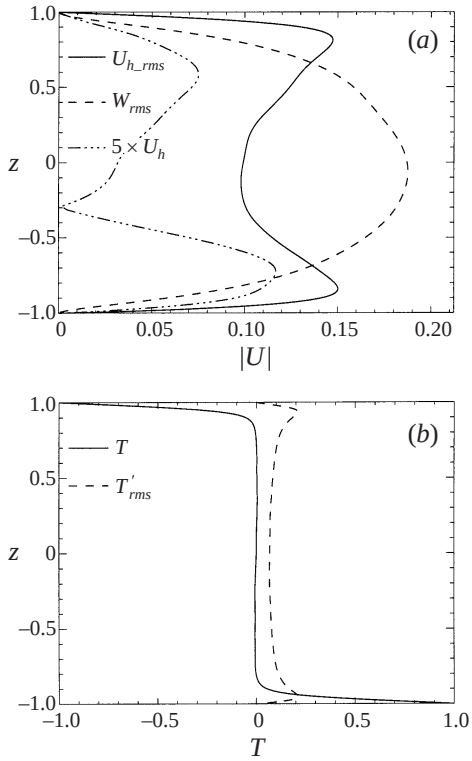

FIGURE 4. Profiles of (*a*) root-mean velocities U_{h_rms}(——), $W_{rms}(- - -) = (\overline{u^2})^{1/2}, (\overline{w^2})^{1/2}$, and the mean horizontal velocity $U_h = |\overline{u}|(- \cdot -)$ in the direction of maximum mean flow; (*b*) temperature variance $T'_{rms} = (\overline{T'^2})^{1/2}(- - -)$ and temperature $\overline{T}$(——) for a single time from the $Pr = 7$, $Ra = 10^7$ calculation.

order of scaling for $Pr < 0.07$ and $Ra \sim 10^7$. Since the low-Pr order of boundary layer thicknesses is different from the order for $Pr = 0.7$, this would suggest the possibility of a different scaling for Nu versus Ra for low Pr and $Ra \sim 10^7$. This is consistent with the $\beta_T \approx 0.26$ in figure 1(*a*) for $Pr = 0.07$ and $\beta_T \approx 0.25$ in the mercury $Pr = 0.025$ experiments (Cioni *et al.* 1997) instead of $\beta_T = 2/7 \approx 0.28$. Would a crossover to $2/7$ be expected for $Pr = 0.07$? The trends for λ_u and λ_T are such that a crossover would be expected for $Ra \approx 8 \times 10^6$, just beyond the currently computable range.

An alternative to calculating higher Ra in order to see a crossover is to do a series of calculations for a higher Pr where the crossover would be within the range of Ra that can be simulated. Initially the $Pr = 0.7$ data were considered as such a case. For $Pr = 0.7$ there is a crossover from $\lambda_u < \lambda_T$ to $\lambda_u > \lambda_T$ between $Ra = 10^4$ and 10^5 and there is also a slight change in the $Nu \sim Ra^{\beta_T}$ scaling, from $\beta_T < 0.28$ for $Ra < 5 \times 10^4$ to $\beta_T = 0.28$ for $Ra > 5 \times 10^4$. However, this transition is not significant enough and at too low a Rayleigh number to be a convincing example for such a transition.

This is what inspired the extra set of $Pr = 0.3$ calculations reported here. For $Pr = 0.3$ in figure 2(*b*) there is a crossover from $\lambda_u < \lambda_T$ for $Ra < 4 \times 10^5$ to $\lambda_u > \lambda_T$ for $Ra > 4 \times 10^5$. This is where a change in scaling from $\beta_T \approx 0.26$ for $Ra < 4 \times 10^5$, to $\beta_T \approx 0.28$ for $Ra > 4 \times 10^5$ was noted in figure 1(*b*). Therefore, in this case the

crossovers would be consistent with a transition from $Nu \sim Ra^{1/4}$ to $Nu \sim Ra^{2/7}$ once the order $\lambda_u > \lambda_T > z^*$ appears. The implications for mercury $Pr = 0.025$ are given below.

For $Pr = 7$, there is a crossover from z^* greater than both λ_T and λ_u for low Ra to $z^* < \lambda_T < \lambda_u$ at $Ra = 2 \times 10^5$. Consistent with this, $\beta_T \approx 0.28$ for $Ra > 2 \times 10^5$ and $\beta_T < 0.28$ for $Ra < 2 \times 10^5$ is plausible in figure 1(*c*). There are some experiments in water (Chu & Goldstein 1973) that find $\beta_T < 2/7$ and a new experiment by Xu, Bajaj & Ahlers (2000) for $Pr = 4$ that is consistent with $\beta_T < 2/7$ for low Ra. The observation here that the order $z^* < \lambda_T < \lambda_u$ does not appear for $Ra < 2 \times 10^5$ makes it plausible that for high Pr, $\beta_T \neq 2/7$ if Ra is small. However, without some higher-Pr results that show $z^* > \lambda_T$ and $z^* > \lambda_u$ and a longer anomalous range in Nu, it is impossible to determine if this small change is significant or due to the small Reynolds number at this Ra and Pr.

Figure 2(*d*) plots z^*, λ_T and λ_u as a function of Pr. As in figure 1(*d*), the 10^7 values for $Pr = 0.07$ are extrapolated values and small changes in these extrapolated values would not change the conclusions about crossovers. The scaling with Pr of the three thicknesses are approximately $z^* \sim Pr$, $\lambda_T = 0.5/Nu \sim Pr^{-0.12}$ for $Pr < 0.3$ and nearly constant for $Pr > 1$, and $\lambda_u \sim Pr^{0.21}$. Crossovers as a function of Pr are predicted for $Ra = 10^7$ near $Pr = 0.07$ and perhaps near $Pr = 20$ for a transition to $z^* > \lambda_T$ and λ_u. Figure 2(*d*) and the Ra trends in figure 2(*a–c*) can be used to predict the Ra when a crossover to $z^* < \lambda_T < \lambda_u$ occurs for any Pr. For mercury ($Pr = 0.025$), the prediction is that $z^* < \lambda_T < \lambda_u$ would develop at $Ra = 3 \times 10^8$, at the upper end of the experimental measurements (Cioni *et al.* 1997). Therefore, for $Ra < 10^9$, one would not expect these experiments to have shown a $2/7$ scaling. We would predict a $Nu \sim Ra^{2/7}$ regime if a long enough regime for $Ra > 3 \times 10^8$ could be observed. We have just become aware of new evidence for the transition predicted here in a mercury experiment by Glazier *et al.* (1999) for Ra up to 8×10^{11}.

6. Large-scale flow

Knowing how the Rayleigh and Prandtl numbers and any of the crossovers discussed above affect the large-scale flow is necessary if we are to understand the scaling physics. Recall that large-scale flows are one hypothesized source of the velocity boundary layer that is believed to be responsible for the $2/7$ scaling. Time series of laser lines for aspect ratio $W/D = 12$ and $Pr = 6.7$ show evidence of a transition to a large-scale flow for this range of Ra (Krishnamurti & Howard 1981). For $Ra = 10^6$, the patterns were elongated in x and without any slant, suggesting a series of roll patterns passing by. For $Ra = 2.6 \times 10^6$, the patterns were more discontinuous and were slanted, indicating a preferred direction to the flow and perhaps a large-scale sweeping pattern that was explained by a bootstrap model (Howard & Krishnamurti 1986). In large-aspect-ratio simulations for $Pr = 0.7$ with periodic sidewalls (Kerr 1996), a large-scale flow results from several large-aspect-ratio convection cells. This section will discuss the changes associated with using impenetrable sidewalls, the dependence on Pr, and what evidence there is in structures for the reported transitions in scaling.

Low Prandtl number results are discussed first. These are qualitatively similar to earlier visualizations for $Pr = 0.7$ (Kerr 1996). Then we discuss what evidence there is for changes in flow patterns in the high Prandtl number regime. The conclusion will be that there are distinct differences in the large-scale structures between the largest and smallest Prandtl numbers of these simulations, but distinct changes in the

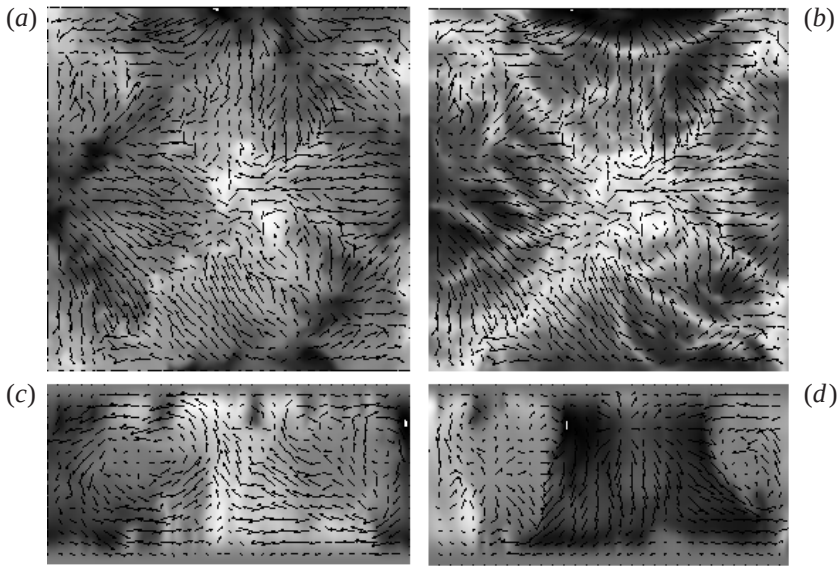

FIGURE 5. Cross-sections of fluctuation temperature $T' = T - \overline{T(z)}$ for the $Pr = 0.07$, $Ra = 2 \times 10^6$ calculation. The slices shown are (*a*) a horizontal slice through the centre, (*b*) a horizontal slice through the boundary layer, (*c*) a vertical slice through the centre and (*d*) a vertical slice on one sidewall. The scale of each slice is the maximum (white) and minimum (black) in that slice.

flow as a function of Rayleigh number are less obvious. Many of the conclusions are subjective and incomplete, so figures for a continuous range of Pr are included to allow the readers to come to their own conclusions.

Figures 5, 7, 8 and 9 show greyscale contour slices of the fluctuation temperature $T' = T - \overline{T}(z)$ for the highest Rayleigh numbers for $Pr = 0.07$, 0.3, 2 and 7 respectively. In addition, figure 6 shows greyscale contours of the vertical velocity w to show how turbulent the field is at low $Pr = 0.07$. Figure 10 shows T' greyscale contours for a lower Rayleigh number $Ra = 10^6$ for $Pr = 7$ because this is the Pr for which changes in structure as Ra is increased were found experimentally (Krishnamurti & Howard 1981). $Pr = 0.7$ is not shown because the structures are little different from those reported earlier (Kerr 1996) and because the major features are represented by $Pr = 0.3$. $Pr = 4$ is not shown because the trend with increasing Pr is adequately represented by $Pr = 2$ and 7. The shading scale in each slice is between the maximum (white) and minimum (black) values in that slice. These values can be inferred from the profiles in figures 3 and 4 and the inverse Reynolds numbers and Nusselt numbers that appear as length scales in figure 2.

The slices shown for each field are a horizontal slice through the centre, a horizontal slice through the boundary layer, a vertical slice through the centre and a vertical slice on one sidewall. The slices through the boundary layers are taken roughly halfway between the position of the peaks of U_{h_rms} and T'_{rms} such as in figures 3 and 4. The vertical slices are plotted on a 4×2 domain, although the physical domain is 4×1. Vertical slices have also not been remeshed onto a uniform grid from the original Chebyshev mesh, so boundary layers appear thicker in proportion to the rest of the flow than they are. For $Pr = 0.07$ and $Pr = 7$ ($Ra = 10^7$), velocities in the planes are shown with arrows to demonstrate what types of large-scale flows and structures are typical in these simulations.

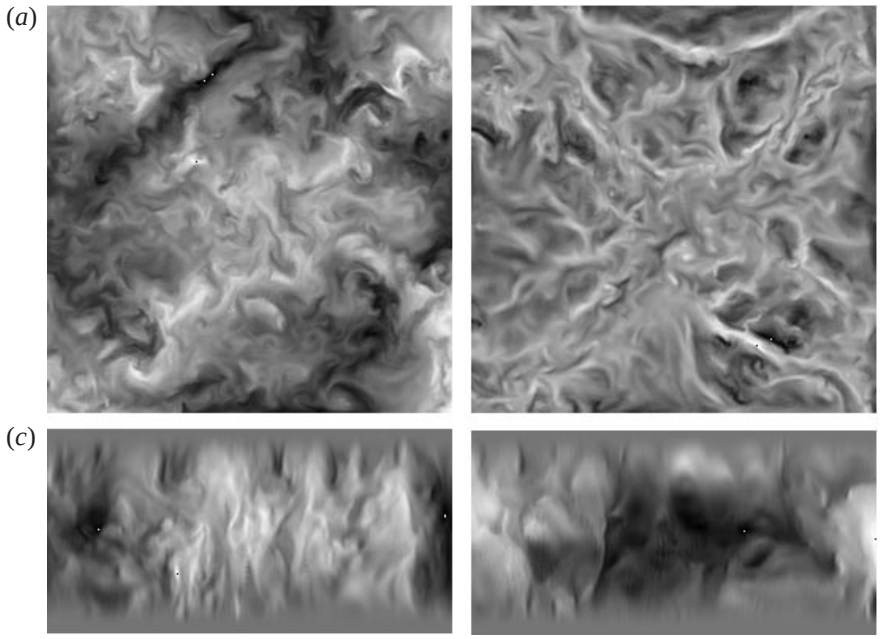

FIGURE 6. Cross-sections, as in figure 5, of vertical velocity w for the $Pr = 0.07$, $Ra = 2 \times 10^6$ calculation.

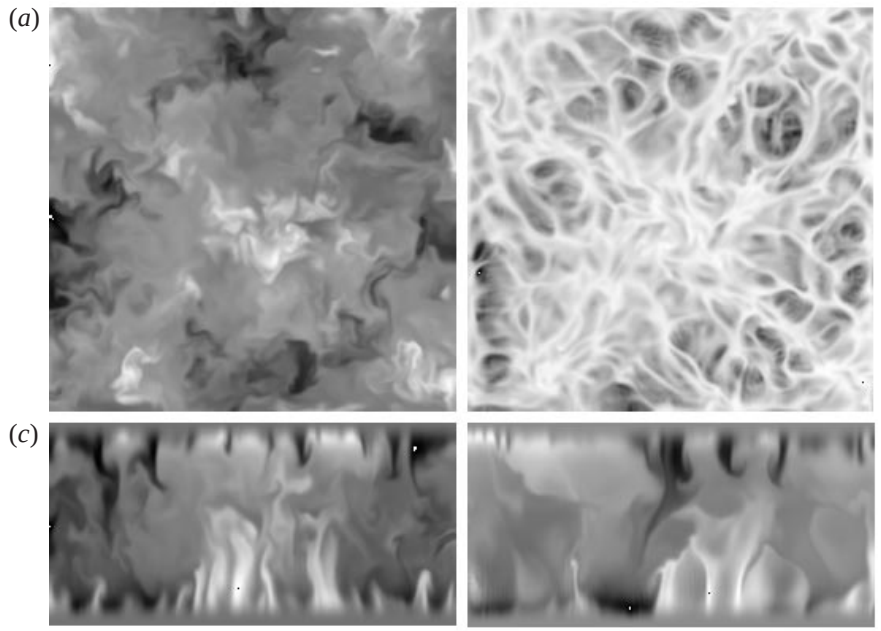

FIGURE 7. Cross-sections, as in figure 5, of fluctuation temperature $T' = T - \overline{T(z)}$ for the $Pr = 0.3$, $Ra = 10^7$ calculation.

In earlier work for $Pr = 0.7$ and periodic sidewalls (Kerr 1996), the entire flow outside the boundary layers was dominated by a few large-scale convective cells, while in the boundary layer there is a fine network of thin, extended plumes concentrated on the large-scale pattern. A series of vertical slices in time showed the fine-scale networks

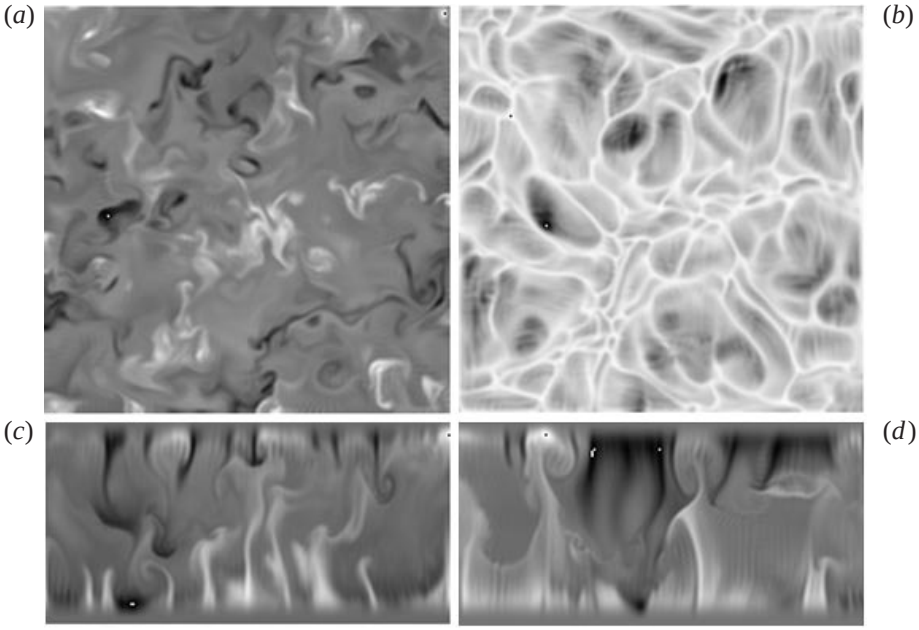

FIGURE 8. Cross-sections, as in figure 5, of fluctuation temperature $T' = T - \overline{T(z)}$ for the $Pr = 2$, $Ra = 10^7$ calculation.

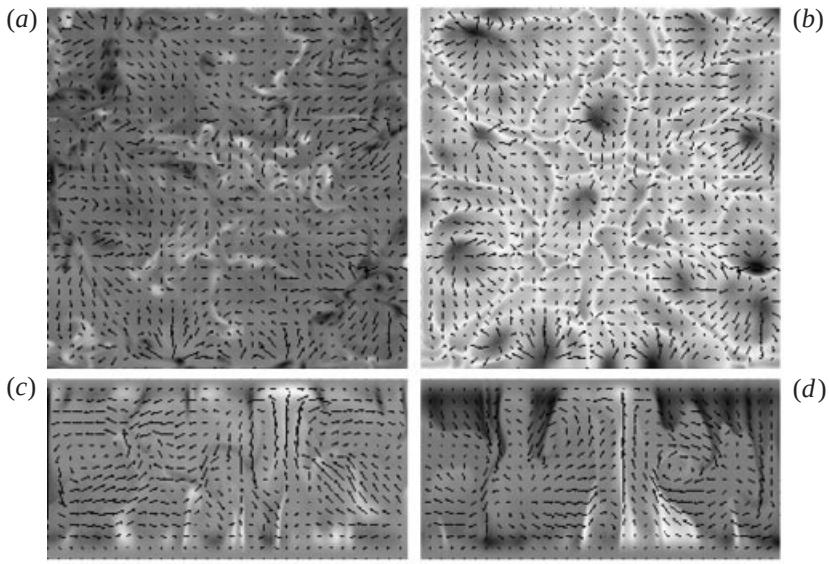

FIGURE 9. Cross-sections, as in figure 5, of fluctuation temperature $T' = T - \overline{T(z)}$ for the $Pr = 7$, $Ra = 10^7$ calculation.

being swept intermittently into the large-scale patterns that dominate the rest of the flow. The large-scale patterns through the centre were conglomerations of thin plumes originating in the boundary layer. The patterns did not change qualitatively as Ra was increased except that plumes through the interior become thinner, networks near

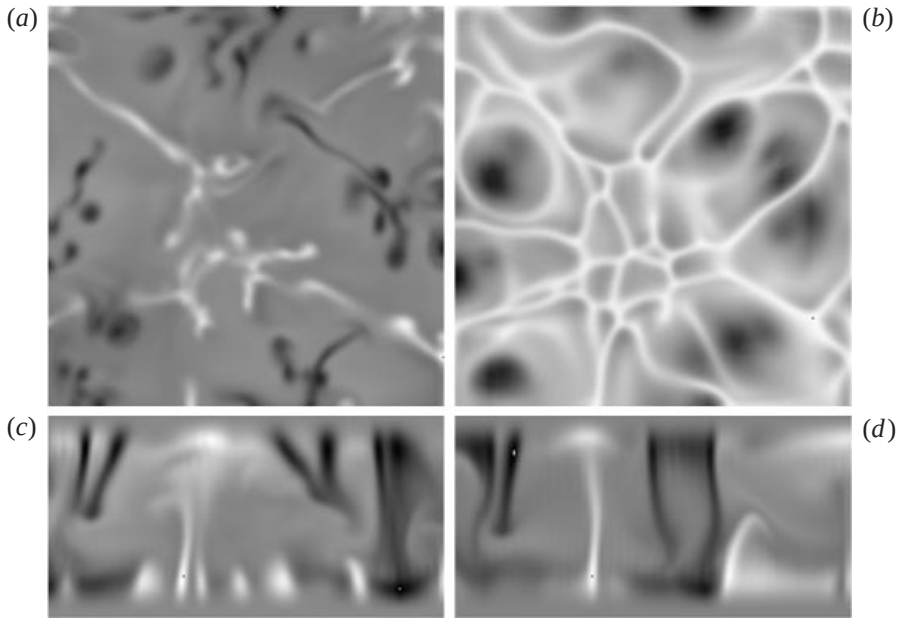

FIGURE 10. Cross-sections of fluctuation temperature $T' = T - \overline{T(z)}$ for the $Pr = 7$, $Ra = 10^6$ calculation.

the boundaries were better defined, and the flow became more tangled and knotted around vortex cores as it became more turbulent.

The horizontal slices for $Pr = 0.07$ and 0.3 in figures 5 and 7 show patterns that are in many ways qualitatively similar to those seen previously for $Pr = 0.7$. Figure 8 for $Pr = 2$ also shows some of these features and is included in the following discussion to demonstrate the dependence of Pr. With free-slip instead of periodic sidewalls, the results for $Pr = 0.07$ to 0.7 show a dominant crossing pattern of one sign in the centre of the centre horizontal slice that is particularly obvious in vertical velocity, with compensating lanes of the opposite sign nearer the corners. In the corners themselves are plumes of the same sign as in the centre. The patterns of networks in the boundary layers converge upon the interior patterns. In the boundary layer, as Pr decreases from 2 to 0.3, the fine networks in temperature near the surfaces become denser and thicker, perhaps due to increasing Reynolds number. Vertical slices such as in figures 8(c) and 7(c) show how the individual plumes rising out of these boundary layer patterns are becoming more bunched together as Pr decreases. Slices of vertical velocity for $Pr = 2$ and 0.3 follow the same pattern.

These trends are not continued for T' for $Pr = 0.07$ in figure 5, where smoothing by the increased thermal diffusivity seems to be winning over the greater complexity that would be caused by the increased Reynolds number. Associated with the broader temperature structures in the boundary layer for $Pr = 0.07$ in figure 5(b), the plumes in the vertical slices of T' for $Pr = 0.07$ in figure 5(c) are much smoother than those for $Pr = 0.3$ in figure 7(c). The large-scale flow indicated by the arrows in figure 5(c) is two large-scale cells. The use of arrows suggests smooth variations in the velocity. Figure 6 displays slices of vertical velocity to indicate that there is an underlying fine-scale turbulent flow. For $Pr = 0.07$ the bunching together of fine vertical motions has expanded until the bunches uniformly fill the entire domain in figure 6(c). This fine structure extends to the top of the boundary layers, that is the

peak of the T'_{rms} and U_{h_rms} profiles in figure 3. In the vertical slices at the wall in figures 5(d) and 6(d), the dominant pattern is flow coming into the wall at midlevel, and then moving up or down. Motions at the vertical walls do not extend from bottom to top in conjunction with plumes, but are dominated by forcing from the interior.

Given the crossover in boundary length scales for $Pr = 0.3$ in figure 2(b), it might be expected that patterns would be different for $Pr = 0.3$ at $Ra = 10^7$ and $Pr = 0.07$ at $Ra = 2 \times 10^6$ because they are in different regimes. It might also be expected that $Pr = 0.3$ patterns for $Ra < 4 \times 10^5$ and $Ra > 4 \times 10^5$ would be qualitatively different because they are in different regimes and that there would be some similarity between $Pr = 0.3$ at $Ra \approx 10^5$ and those for $Pr = 0.07$ at $Ra = 2 \times 10^6$ because they are in the same regime. Perhaps the more diffusive temperature structures in figure 5 and the way velocity structures fill the entire domain in figure 6 represent this transition, but there are no other pattern changes that could be associated with the crossover in length scales. Patterns for $Pr = 0.3$ at $Ra = 10^5$ look more like $Pr = 0.3$ at $Ra = 10^7$ than $Pr = 0.07$ and there are no qualitative differences between individual velocity structures for $Pr = 0.07$ in figure 6 and those for $Pr = 0.3$, where velocity patterns are similar to the temperature patterns in figure 7.

Now we will consider $Pr > 1$. Figures 8 and 9 show temperature slices for $Pr = 2$ and 7 at $Ra = 10^7$, with arrows in figure 9 to show the large-scale flow. Patterns of vertical velocity motions closely follow the temperature patterns, so there is no need to include separate vertical velocity contours.

For $Pr = 2$ and 7, there are large-scale patterns associated with the boundaries that appear in the horizontal slices through the centre, but they are different from the crossing lanes seen for $Pr = 0.07$ and 0.3. As Pr increases in the boundary layer, the horizontal patterns change gradually from what are being called networks to the appearance of convective cells. The vertical slices for $Pr = 2$ and 7 do not show bunches of plumes, rather they show that horizontal boundaries send individual plumes into the interior that are often swept by the local mean motion and tend to be tilted. An example would be around the swirling to the right centre of figure 9(d). A cold plume to the right of the swirl is being swept and tilted to the right towards the right-hand wall by a large-scale sweeping indicated by the arrows. A hot plume to the left of the swirl is being swept and tilted to the left towards the central plume. The term 'mushroom caps' could be used to describe the sweeping and tilting. The sweeping motions observed in our simulations, while not encompassing the entire domain as once believed, do support the basic theoretical interpretation that shears and sweeping motions are related to the $Nu \sim Ra^{2/7}$ scaling. However we should note that other experiments with screens to prevent sweeping seem also to have the 2/7 scaling (Xia & Liu 1997), as well as experiments with rough surfaces (Shen, Tong & Xiu 1996; Du & Tong 1998).

In being swept, these individual plumes tend not to cross the entire domain, although their penetration into the interior seems to be much greater than the thermal boundary layer thickness. In the vertical slices through the centre in figures 8(c) and 9(c), there are no plumes that penetrate from boundary to boundary. Even on the vertical wall in figures 8(d) and 9(d), only a few plumes penetrate. The result is that, unlike $Pr = 0.07$ and 0.3, no signature of the boundary layer patterns seems to persist into the centre horizontal slice at $Pr = 7$.

Could these tilted structures be associated with the laser line patterns observed in the water tank experiments (Krishnamurti & Howard 1981)? They could be, if the experiments were interpreted as evidence for localized sweeping patterns rather than

for flows sweeping across the entire domain. Tilted plumes like those in figure 9(*d*) would also be consistent with water tank visualizations (Wu & Libchaber 1992).

Recall that the laser line experiments also showed a transition in structure between $Ra = 10^6$ and $Ra = 2.6 \times 10^6$ (Krishnamurti & Howard 1981). For $Pr = 7$ and a lower $Ra \approx 10^5$, a crossover in length scales is seen in figure 2(*c*) and a minor change in the scaling of Nu with Ra is seen in figure 1(*c*). In order to be more faithful to the experimental laser strip pictures, time series of strips of temperatures and velocities were taken while these calculations were running and stored for later use. Analysis of these time series has yet to be done, so for now, to determine if there is an analogous transition in the structure, figure 10 shows temperature slices for $Pr = 7$ and 10^6, which is the lowest Ra for $Pr = 7$ that could be considered turbulent. A stronger relationship to the boundaries can be seen, with plumes through the centre that are connected to the boundaries and some element of the crossing pattern that appears at lower Pr. However, a tendency for plumes to be tilted and probably swept by the local mean flow, is also observed for $Ra = 10^6$ in figure 10(*d*). Therefore, the best conclusion is that unlike the laser lines in the water tank experiment (Krishnamurti & Howard 1981), a significant change in structure is not observed.

It was first reported that for the $Pr = 7$, $Ra = 10^5$ simulations (Kerr *et al.* 1995) the maximum mean horizontal velocity $\max[U_h(z)]$ in one direction was the order of 0.2 times the maximum of the root-mean velocity $\max[U_{h\_rms}(z)]$, whereas the maximum mean velocities in the other direction is three times smaller. In addition, a visualization using velocity arrows showed a large-scale sweeping pattern across one wall. We have not found an example of such sweeping across a wall in any of the higher-Ra calculations reported here; however figure 4(*a*) shows a mean velocity profile U_h for $Pr = 7$ that is consistent with the lower-Ra result of Kerr *et al.* (1995). The maximum of U_h with respect to the maximum of U_{h_rms} is about twice the maximum for $Pr = 0.07$ in figure 3(*a*).

7. Discussion

The primary result of this paper is that for the entire range of Prandtl numbers studied, there is always a crossover in length scales such that the order and scaling with Rayleigh number of three boundary layer thicknesses obey $z^* < \lambda_T < \lambda_u$ and that once this regime is obtained that $Nu \sim Ra^{\beta_T}$ with $\beta_T \approx 2/7$ is found. The scaling with Ra of the three thicknesses in this regime for all Pr is consistent with earlier results (Kerr 1996) for $Pr = 0.7$ where $z^* \sim Ra^{-3/7}$, $\lambda_T \sim Ra^{-2/7}$ and $\lambda_u \sim Ra^{-1/7}$.

When some order other than $z^* < \lambda_T < \lambda_u$ is found, is a different Nusselt number scaling obtained? Crossovers in these length scales for $Pr = 0.3$ and $Pr = 7$ are associated with small changes in the Nu versus Ra scaling, in particular the crossover to $\lambda_u < \lambda_T$ for low Prandtl number could explain the $Nu \sim Ra^{1/4}$ for the $Pr = 0.07$ simulations and $Pr = 0.025$ mercury experiments (Cioni *et al.* 1997). Crossovers to $2/7$ behaviour in Nu are predicted to be just beyond the maximum Ra simulated for $Pr = 0.07$ and we have just learned that our predicted change to $2/7$ for mercury $Pr = 0.025$ has been observed (Glazier *et al.* 1999). The prediction for $Pr \equiv 0$ would be that the $2/7$ regime would never be reached and results at low Pr and moderate Ra might be relevant (Thual 1992; Spiegel 1962). High-Pr results are consistent with a slight decrease in Nu in experiments between $Pr = 4$ and 7 and are therefore consistent with the experiments showing a slower decrease than predicted (Liu & Ecke 1997; Niemela *et al.* 2000).

The crossovers with Ra for given Pr seem to be associated only weakly with

changes in flow structure. However, there are significant changes in structure between the smallest and largest Pr simulated. At large Pr, structures through the horizontal centre of the flow are not strongly aligned with the geometry of the domain or with clearly defined boundary layer cells. Only isolated plumes are observed that are swept by intermediate-scale flows. At intermediate Pr, the structures through the horizontal centre become aligned with the geometry and the cells in the boundary layer turn more into networks that are composed of plumes that are being swept into the larger-scale patterns between the boundary layers. The structures through the centre could be characterized as chimneys containing conglomerations of plumes and isolated plumes disappear. At very low Pr, the networking remains, but the sweeping in the boundary layers is less obvious and the conglomerations of plumes cannot be separated easily into separate chimneys.

Overall, the clearest change in structure with Pr is from aggregates of plumes for $Pr \leqslant 1$ to individual plumes for $Pr > 1$. Since at $Ra = 10^7$ all the crossovers to $z^* < \lambda_T < \lambda_u$ have occurred for $0.3 < Pr < 7$, there is no obvious source for this structural change.

Many of the issues studied here and in Kerr *et al.* (1995) have also been studied in a new paper by Verzicco & Camussi (1999). The main differences in the flow configuration are that they used aspect ratio 1, a cylindrical geometry, and no-slip sidewalls. Further work on the differences due to $A = 1$ is under way (Kerr *et al.* 2000). The Rayleigh number of Verzicco & Camussi (1999) was slightly lower and they studied $Pr = 0.022$ for mercury. The conclusions about different flow regimes at low Pr, which is dominated by thermal diffusivity and large-scale flow, and high Pr, which is dominated by individual plumes, are similar, although we have emphasized the role of fine-scale turbulence at low Pr more. Their conclusions concerning crossovers are different, largely because their velocity boundary layer thickness was neither z^* nor λ_u.

The primary conclusion is that calculations at several Prandtl numbers all support the suggestion by Kerr (1996) that the trends in boundary length scales are consistent with $Nu \sim Ra^{\beta_T}$, $2/7 \leqslant \beta_T \leqslant 0.309$ being the only asymptotic high Rayleigh number scaling regime for all finite Pr. This suggestion is now supported experimentally at Ra up to 10^{17} in a helium tank (Niemela *et al.* 2000) and in mercury for Ra up to 8×10^{10} (Glazier *et al.* 1999). In the helium experiment, as noted above, the data are actually reported to be more consistent with $Nu \sim Ra^{0.309}$, with $Ra^{2/7}$ ruled out. However, it is not clear to what extent the small aspect ratio modifies the exponent. The empirical observations given here linking z^*, λ_T and λ_u have only partial theoretical support. The current theories predict either z^* (Shraiman & Siggia 1990) or λ_u (Castaing *et al.* 1989), but not both. These observations should encourage the theoretical community to reconsider their theories and try to explain why both z^* and λ_u appear to play dynamical roles.

NCAR is sponsored by the National Science Foundation. Input from S. Ciliberto, R. Ecke and M. Rast is appreciated. The major results were first presented at a symposium in Los Alamos in May 1998 to honor R. H. Kraichnan.

REFERENCES

Ashkenazi, S. & Steinberg, V. 1999 High Rayleigh number turbulent convection in a gas near the gas–liquid critical point. *Phys. Rev. Lett.* (submitted).

Belmonte, A., Tilgner, A. & Libchaber, A. 1994 Temperature and velocity boundary layers in turbulent convection. *Phys. Rev.* B **50**, 269–279.

Castaing, B., Gunaratne, G., Heslot, F., Kadanoff, L., Libchaber, A., Thomae, S., Wu, X. Z.,

Zaleski, S. & Zanetti, G. 1989 Scaling of hard thermal turbulence in Rayleigh–Bénard convection. *J. Fluid Mech.* **204**, 1–30.

Chandrasekar, S. 1961 *Hydrodynamic and Hydromagnetic Stability*. Clarendon.

Chavanne, X., Chillà, F., Chabaud, B., Castaing, B., Chaussy, J. & Hébral, B. 1996 High Rayleigh number convection with gaseous helium at low temperature. *J. Low Temp. Phys.* **104**, 109–129.

Chu, T. Y. & Goldstein, R. J. 1973 Turbulent convection in a horizontal layer of water. *J. Fluid Mech.* **60**, 141–159.

Cioni, S., Ciliberto, S. & Sommeria, J. 1997 Strongly turbulent Rayleigh–Bénard convection in mercury: comparison with results at moderate Prandtl number. *J. Fluid Mech.* **335**, 111–140.

DeLuca, E. E., Werne, J., Rosner, R. & Cattaneo, F. 1990 Numerical simulations of soft and hard turbulence: preliminary results for two-dimensional convection. *Phys. Rev. Lett.* **64**, 2370–2373.

Du, Y.-B. & Tong, P. 1998 Enhanced heat transport in turbulent convection over a rough surface. *Phys. Rev. Lett.* **81**, 987–990.

Glazier, J. A., Segawa, T., Naert, A. & Sano, M. 1999 Evidence against 'ultrahard' thermal turbulence at very high Rayleigh numbers. *Nature* **398**, 307–310.

Goldstein, R. J., Chiang, H. D. & See, D. L. 1990 High-Rayleigh-number convection in a horizontal enclosure. *J. Fluid Mech.* **213**, 111–126.

Herring J. R. 1966 Some analytic results in the theory of thermal convection. *J. Atmos. Sci.* **23**, 672–677.

Herring, J. R. 1969 Statistical theory of thermal convection at large Prandtl number. *Phys. Fluids* **12**, 39–52.

Herring, J. R. & Jackson, S. 1984 Thermoconvection: numerical experiments near the onset to turbulence and the statistical theory of turbulence. In *Turbulence and Chaotic Phenomena in Fluids* (ed. T. Tatsumi) pp. 111–116. North-Holland.

Heslot, F., Castaing, B. & Libchaber, A. 1987 Transition to turbulence in helium gas. *Phys. Rev.* A **36**, 5870–5873.

Howard, L. N. & Krishnamurti, R. 1986 Large-scale flow in turbulent convection: a mathematical model. *J. Fluid Mech.* **170**, 385–410.

Julien, K., Legg, S., McWilliams, J. & Werne, J. 1996 Hard turbulence in rotating Rayleigh–Bénard convection. *Phys. Rev.* B **53**, 5557–5560.

Kerr, R. M. 1996 Rayleigh number scaling in numerical convection. *J. Fluid Mech.* **310**, 139–179.

Kerr, R. M., Brandenburg, A. & Herring, J. R. 2000 Small length scales in hard convective turbulence. In preparation.

Kerr, R. M., Herring, J. R. & Brandenburg, A. 1995 Large-scale structure in Rayleigh–Bénard convection with impenetrable side-walls. *Chaos, Solitons and Fractals* **5**, 2047–2053.

Kim, J., Moin, P. & Moser, R. 1987 Turbulence statistics in fully developed channel flow at low Reynolds number. *J. Fluid Mech.* **177**, 133–166.

Krishnamurti, R. & Howard, L. N. 1981 Large-scale flow generation in turbulent convection. *Proc. Natl Acad. Sci.* **78**, 1981–1985.

Liu, Y. & Ecke, R. 1997 Heat transport scaling in turbulent Rayleigh–Bénard convection: effects of rotation and Prandtl number. *Phys. Rev. Lett.* **79**, 2257–2260.

Lohse, D. & Grossman, S. 2000 Scaling in thermal convection: a unifying theory. *J. Fluid Mech.* **407**, 27–56.

Niemela, J. J., Skrbek, L., Sreenivasan, K. R. & Donnelly, R. J. 2000 Turbulent convection at very high Rayleigh numbers. *Nature* **404**, 837–840.

Sano, M., Wu, X. Z. & Libchaber, A. 1989 Turbulence in helium-gas free convection. *Phys. Rev.* A **40**, 6421–6430.

Shen, V., Tong, P. & Xiu, K.-Q. 1996 Turbulent convection over rough surfaces. *Phys. Rev. Lett.* **76**, 908–911.

Shraiman, B. I. & Siggia, E. D. 1990 Heat transport in high-Rayleigh-number convection. *Phys. Rev.* A **42**, 3650–3653.

Spiegel, E. D. 1962 Thermal turbulence at very small Prandtl number. *J. Geophys. Res.* **67**, 3063–3070.

Thual, O. 1992 Zero Prandtl number convection. *J. Fluid Mech.* **240**, 229–258.

Verzicco, R. & Camussi, R. 1999 Prandtl number effects in convective turbulence. *J. Fluid Mech.* **383**, 55–73.

Werne, J. 1993 Structure of hard-turbulent convection in two dimensions: Numerical evidence. *Phys. Rev.* B **48**, 1020–1035.

Werne, J., DeLuca, E. E., Rosner, R. & Cattaneo, F. 1991 Development of hard–turbulent convection in two dimensions: numerical evidence. *Phys. Rev. Lett.* **67**, 3519–3522.

Wu, X.-Z. & Libchaber, A. 1992 Scaling relations in thermal turbulence: The aspect-ratio dependence. *Phys. Rev.* A **45**, 842–845.

Xia, K.-Q. & Liu, S.-L. 1997 Turbulent thermal convection with an obstructed sidewall. *Phys. Rev. Lett.* **79**, 5006–5009.

Xu, X., Bajaj, K. & Ahlers, G. 2000 Heat transport in turbulent Rayleigh–Bénard convection. *Phys. Rev. Lett.* **84**, 4357–4360.

Zocchi, G., Moses, E. & Libchaber, A. 1990 Coherent structures in turbulent convection, an experimental study. *Physica* A **166**, 387–407.